JOURNAL OF AIRCRAFT
Vol. 47, No. 6, November–December 2010

Load Alleviation on a Joined-Wing Unmanned Aircraft

Nicola Paletta,* Marika Belardo,† and Modesto Pecora‡
Centro Italiano Ricerche Aerospaziali, 81043 Capua, Italy

DOI: 10.2514/1.C000265

In this paper a method of alleviating wing structural load of a flexible aircraft during a symmetric balanced maneuver is presented. An application on the unmanned aircraft in development at the Italian Aerospace Research Center, high-altitude performance demonstrator, characterized by a joined-wing configuration, is illustrated. This load alleviation technique enables a desired value of the bending moment on a fixed wing control station to be obtained. The load reduction is achieved by deflecting a suitable set of flight-control surfaces, by always keeping the vertical load factor constant to preserve the maneuvering performance. The main hypotheses are: significant aeroelastic effects, linear behavior of aerodynamics and structure, and unvarying tensor of inertia under structural deflections. High-altitude performance demonstrator is a scaled performance demonstrator of an 80*m*-wing span high-altitude and long endurance unmanned aircraft in a joined-wing configuration. The advantages in terms of performance, fatigue life extension, and weight reduction can be achieved from the integration of an onboard load alleviation system. The results show that the attainable value of load alleviation in terms of bending moment reduction at the wing root is 37%. Moreover, the test-case analyses show that the maximum value of the alleviation increases with respect to the dynamic pressure although the load distribution varies because of significant aeroelastic effects.

Nomenclature

C_m = aerodynamic pitching moment coefficient
$C_{m'}$ = local (strip) moment coefficient
$C_{n'}$ = local (strip) lift coefficient
C_Z = aerodynamic force coefficient along z direction
c_r = aeroelastic reference chord
$\underline{F}_a$ = forces evaluated on the aerodynamic boxes
$\underline{F}_{st}$ = forces evaluated on interchange data grids
G = control function
m = generalized masses
n_z = limit vertical load factor
$\tilde{P}$ = quasi-steady aerodynamic pressure
$\underline{\underline{Q}}$ = generalized aerodynamic forces
$\underline{q}$ = vector of generalized degrees of freedom
q = dynamic pressure
q_i = generalized degree of freedom associated with mode i
S = reference wing surface
$\underline{u}_a$ = vector of local displacements evaluated on the aerodynamic boxes
$\underline{u}_{st}$ = vector of local displacements evaluated on interchange data grids
V = aircraft velocity
V_A = design maneuvering speed
V_C = design cruising speed
V_D = design dive speed
V_S = stalling speed
α = angle of attack
δ = elevator deflection
β = load alleviation control surface deflection
ρ = air density
ϕ_i^x = generic modal amplitude due to mode i along x direction
ϕ_i^y = generic modal amplitude due to mode i along y direction
ϕ_i^z = generic modal amplitude due to mode i along z direction
$\underline{\underline{\Theta}}_{a,st}$ = interpolation matrix

Received 18 January 2010; revision received 2 July 2010; accepted for publication 22 July 2010.

*Aerospace Researcher, Aero-Structural Design and Analysis Group; n.paletta@cira.it.
†Aerospace Researcher, Aero-Structural Design and Analysis Group; m.belardo@cira.it.
‡Technical Supervisor for Aeroelasticity and Project Manager, Aeronautical Program Office; m.pecora@cira.it.

I. Introduction

OVER the last few decades, several kinds of load alleviation systems have been studied and installed on aircraft. These load alleviation systems are mainly aimed at gust-alleviation for improved ride comfort, e.g., Boeing 747 and Lockeed L-1011. The alleviation is accomplished by means of an active wing bending damping, which alleviates structural fatigue loads on the one hand, and lowers pitch attitude variation and vertical accelerations in the cabin on the other [1–3]. A recent survey by Hecker and Hahn [4] showed that a gust-load alleviation system directed toward the reduction of vertical accelerations due to turbulence can yield to an undesired over-compensation of structural loads, which can be avoided only by appealing on an optimized tuning of the gust-load alleviation system: the simulation results from the authors showed good performance also for load alleviation.

Aircraft wing structure is generally maneuver-load or gust-load critical depending on whether the airplane is an unmanned high-performance or a transport airplane. In the case of an unmanned high-performance aircraft the improving of ride comfort is not a concern, whereas a method aimed at reducing directly internal structural loads due to maneuvers is of great significance if the alleviated maneuver can be performed by attaining the same vertical load factor as the unalleviated one.

Several surveys highlighted the advantages achievable with active control systems [5,6] on fighter and/or transport applications: Pratt [5], developed under NASA supersonic transport (SST) Program, reported a structural weight saving of about 1000–2000 lb (referring to NASA SCAT-15F concept) derived from a 5–9% reduction of wing root bending moment. Kurzhals [6] pointed out that active control systems are a useful means to reduce structural weight as well as to decrease direct operational costs related to fuel consumption (15% reduction in wing weight meant 2–3% reduction in direct operational costs) and to enhance fatigue life. The active lift distribution control system installed on an entire C-5 fleet showed

that maneuver and gust incremental wing stresses where reduced to approximately 20–30% with a 1.25 life improvement factor. Recent research work by Caplin et al. [7] was aimed at setting up a design methodology for a robust damage-mitigating control that could achieve structural durability without loss of aircraft performance. Besides the aeroservoelastic model, the damage-mitigating control by Caplin et al. included a fatigue crack damage model. The authors pointed to the fact that it would be advisable to consider such a model during the early stage of design to allow the structural engineers and the control system engineers to simultaneously converge to their individual goals.

Structural weight reduction obtained with load alleviation systems that keep the vertical load factor unvaried allows more payload and/or fuel to be carried because the maximum takeoff weight does not vary.

Work conducted by NASA [8] from May 1977 through June 1979 related to a net airplane Operative Empty Weight reduction equivalent to 2.5% of the wing structural box weight due to a maneuver bending moment alleviation performed by symmetrically deflecting the outboard ailerons.

The present work is focused on a different objective that can be achieved with a load alleviation system: to obtain a reduction in structural internal wing loads for enhanced performance (such as an aerodynamic efficiency increase due to a wing Aspect-Ratio augmentation), structural fatigue life extension, or operative empty weight reduction. The principal difference with the above mentioned gust-load alleviation systems is that the enhancement of performances is accomplished by keeping the same maximum vertical load factor attained during the nonalleviated maneuver.

The driving idea of this survey is to perform a load alleviation by means of a symmetrical actuation of the ailerons or other dedicated control surfaces located close to the wing tip to rearrange the aerodynamic loads. This approach is not new [8–13], but the purpose of this paper is to offer a practical approach to quantify the load alleviation during longitudinal balanced maneuvers taking into account aeroelastic effects, in a relatively effortless and linear manner even if it is applied to an aircraft in an unconventional joined-wing configuration.

Many research efforts have been focused on high-altitude and long endurance (HALE) unmanned aerial vehicles over the past few decades, encompassing different aircraft configurations [14–16], different concepts (aircraft and/or airships [16,17]) and/or power systems [17]. The advantages and areas of application of such platforms were widely discussed [18]: they can act as artificial satellites, thus allowing the same potentiality of use, but at a smaller cost due to their self-launch capability and reusability.

Because of weight restrictions, HALE aircraft are typically characterized by a high aspect ratio flying wing configuration. The high flexibility of this configuration makes the linear theories not relevant for the aeroelastic analysis.

Patil et al. [19] presented the results of a low-order, high-fidelity nonlinear aeroelastic analysis on a high aspect ratio flying wing configuration, which showed how the large deflections experienced lead to significant changes in the aeroelastic behavior of the wing, in particular, changes in the natural frequencies as a function of the tip displacement, ergo changes on the flutter speed.

Patil and Hodges [20] developed a complete nonlinear theoretical methodology for the flight dynamic analysis of a highly flexible flying wing configuration, demonstrating that both the flight dynamic modes and the flexible modes change significantly with respect to those predicted with a linear analysis. The same methodology was used by Raghavan and Patil [21] to study additional trim cases and lateral flight dynamics. The nonlinear gust response was also investigated by Patil [22], both in the time domain and in the frequency domain.

Shearer and Cesnik [23] proposed a modified version of a strain-based approach developed earlier by Cesnik and Brown [24,25] to model the high aspect ratio lifting surfaces, and concluded that linearized approaches can be used to study simple symmetric maneuvers whereas nonlinear structural modeling is essential when studying asymmetric maneuvers.

Notwithstanding this, Patil applied the nonlinear aeroelastic methodology developed in the previous works to a joined-wing configuration too [26], coming to the conclusion that nonlinear analysis results were close to the linear analysis results, due to the fact that such a configuration is much stiffer than a similar single wing: the structural nonlinearities for the joined-wing configuration were quite negligible.

Concerning the many advantages of joined-wing configuration if compared with conventional configurations, Wolkovitch [27] highlighted lighter structural weight, less induced drag and a synergistic predisposition to new technologies (for example the use of composite materials and laminar flow airfoils). In addition Wolkovitch himself and other authors [28,29] outlined how even in the preliminary design phase an integrated methodology involving weight estimation techniques, structural analyses and aeroservoelastic design is mandatory if a reliable design is pursued. A brief consideration of the nonnegligible importance of the junctions stiffness on the aeroelastic behavior or about the impact of the redundant configuration on the load evaluation process [29] are ideal examples of this.

The same remarks were made by Frediani et al. [30] and Frediani [31], who were engaged in an Italian national project (during the period 2000–2002), and who focused on the analysis of the PrandtlPlane configuration, a very efficient joined-wing configuration derived from Prandtl intuition. Multidisciplinary preliminary design studies conducted by Frediani and his colleagues took into account aerodynamic efficiency, maneuverability, structure sizing, and aeroelastic phenomena, such as flutter. The aeroelastic aspect was taken into account in a multilevel structural optimization process aimed at the preliminary wing box weight estimation [32,33].

As explained previously, the joined-wing configuration is a valid alternative to a flying wing configuration for solar powered HALE vehicles, not only for its higher structural stiffness and its larger solar array area but also for the possibility to rely solely on linear analysis [26], thus resulting in a cheaper design process.

Demasi and Livne performed aeroelastic analysis on a joined-wing configuration by means of a nonlinear updated Lagrangian formulation for the structural part [34,35], and their results demonstrated a significant influence of structural nonlinearities on divergence and flutter.

Nevertheless in this work the extent of the structural deformations experienced during balanced maneuver analyses, ergo the extent of geometric structural nonlinearities result in a negligible influence on the quasi-steady aerodynamic pressure calculations.

For all the above considerations, it is believed that for such an unconventional airplane a practical approach which is capable of quantifying the Load alleviation, to identify performance targets of endurance, operational costs and payload embarking capability could be a valuable tool especially during the early stages of design.

II. Methodology

Within the hypothesis of linear aerodynamics, aircraft lift and pitch moment can be broken down into their unit aerodynamic contributions due to zero effect, angle of attack, and unit deflections of all the control surfaces involved during the maneuver. The so-called zero effect represents the aerodynamics acting on the airplane at zero angle of attack without any control surface deflection: it is due to airfoil camber, viscosity and other nonnegligible sources of nonlinearity (i.e., strong compressibility effects such as shock waves, etc.).

Among all the internal load characteristics acting on the wing, the principal bending moment M has been chosen as the load characteristic to be reduced because it commonly drives the design of the main wing structure.

The second hypothesis of the survey consists in having small structural displacements, resulting in an unvarying tensor of inertia. This hypothesis is generally valid for conventional aircraft and also for high aspect ratio aircraft having such a main structural typology that leads to relatively small wing displacements under limit loads.

Under such hypotheses the principal bending moment (M_{EQ}) acting on a generic wing section is broken down as follows:

$$M_{EQ} = M_0 + M_\alpha \alpha + \sum_{i=1}^{N} M_{\delta i}\delta_i + M_{n_z=1} n_z \tag{1}$$

where $M_0, M_\alpha, M_{\delta i}, M_{n_z=1}$ are the bending moment derivatives, each one representing the bending moment at a generic wing section due to each unit aerodynamic and inertial contribution.

Because a symmetric deflection of the ailerons or of another dedicated control surface modifies the aircraft longitudinal balance, the equations of longitudinal equilibrium with load alleviation have to be rewritten. The goal is to develop a method that allows the attainment of a desired reduction of the principal bending moment in a specified wing control station (WCS).

The equilibrium equations in quasi-steady symmetric maneuver without load alleviation have to fulfill the following requirements: 1) zero resultant aircraft normal force (z-direction), and 2) zero resultant aircraft pitching moment.

The aircraft has 2 degrees of freedom or dependent variables: the angle of attack and the elevator deflection. Starting from the longitudinal balance equation system for a rigid aircraft

$$\begin{cases} C_{Z_\alpha}\alpha + C_{Z_\delta}\delta = \frac{n_z W}{Sq} - C_{Z_0} \\ C_{m_\alpha}\alpha + C_{m_\delta}\delta = -C_{m_0} \end{cases} \tag{2}$$

the symmetric balanced maneuver parameters, the angle of attack and the elevator deflection, are known because the limit vertical load factor, the aircraft velocity, the altitude, the Mach number, the center of gravity and the aircraft weight are defined.

The system of Eq. (2) is basically valid also for a flexible aircraft. In this latter case, the aerodynamic derivatives must be evaluated taking into account the aircraft flexibility. The aerodynamic moment derivatives are calculated with the respect to the center of gravity and they are firstly dependent on its position.

Defining an alleviation factor (AF) as

$$M_{\text{IMP}} = (1 - \text{AF}) M_{EQ} \tag{3}$$

the desired value of the bending moment M_{IMP} acting on the WCS may be calculated.

The longitudinal balanced condition with load alleviation is accomplished by solving the following system of equations obtained by adding two new equations to the system (2) and by imposing a desired value of AF (and consequently of M_{IMP})

$$\begin{cases} C_{Z_\alpha}\alpha + C_{Z_\delta}\delta + C_{Z_\beta}\beta & = \frac{n_z Mg}{Sq} - C_{Z_0} \\ C_{m_\alpha}\alpha + C_{m_\delta}\delta + C_{m_\beta}\beta & = -C_{m_0} \\ M_\alpha \alpha + M_\delta \delta + M_\beta \beta & = M_{IMP} - M_{n_z=1} n_z - M_0 \\ \beta - n_z G = 0 \end{cases} \tag{4}$$

where β is the deflection of the wing control surface used as load alleviator.

The fourth equation of the system (4) is uncoupled from the others and it represents a linearized relationship between the load alleviation control surface deflection and the limit vertical load factor. The unknown function G

$$G = f(\text{WCSlocation}, q, n_z, \text{AF}, \text{Mach number}) \tag{5}$$

can provide a preliminary indication for the design of a control system aimed at controlling the load alleviator in real time during an unsteady longitudinal maneuver; G is a first estimation of the gain to be used in a single input, single output (SISO) system to link the vertical load factor (output) to the load alleviator deflection (input). Because the aeroelastic model of a generic airplane is available, from extensive calculations it is possible to build a database with the values of the function G with the respect to flight parameters, WCS, and desired level of alleviation to use them as controller gain. The engineering of the control system lies beyond the scope of this work.

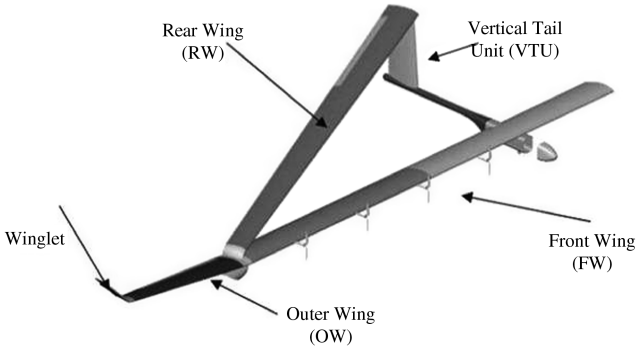

Fig. 1 HAPD primary structures.

III. Application to a Joined-Wing Aircraft

This study has been performed within a research project aimed at the preliminary design of a high-altitude performance demonstrator (HAPD) aimed at performing aerodynamic, structural, flying control experimental tests, and performance demonstration [36].

The joined-wing configuration is a good compromise between high lift, low flexibility and low weight. A potential disadvantage is an increased complexity in the design process. Such a configuration is structurally redundant, resulting in internal forces that depend upon the stiffness distribution. In addition the stiffness of wing junctions has a great influence on the aeroelastic behavior both in terms of divergence and flutter speeds. For these reasons an integrated methodology able to combine the aeroelastic and the structural aspects has been developed at CIRA [29].

The configuration consists of a front wing (FW), including an unswept inner part, an outer part with a negative sweep angle and a winglet tip, and a rear wing (RW) with negative sweep and dihedral angles.

The RW gives additional support to the FW by changing the aerodynamic load distribution and by affecting the wing weight and the structural stiffness distribution. The RW support allows the reduction of FW bending moments and consequently its structural weight. The junction location is at about 70% of the FW semispan, which was chosen as best location as shown by Wolkovitch in [27].

Basic aeroelastic investigations have been introduced early in the design process due to the nonnegligible flexibility of the wing and the elastic-body natural frequencies quite close to the typical flight rigid-body frequencies of the vehicle.

HAPD is characterized by a max takeoff weight of 184.4 kg with the center of gravity located at 81.3% of the FW mean chord. The expected limit vertical load factor is $n_{z\,\text{lim}} = 3.8$, the stalling speed is 14.07 m/s, the design maneuvering speed is 28.94 m/s, the design cruising speed is 33.30 m/s, and the dive speed is 39.00 m/s (see Table 1).

The HAPD primary structures are shown in Fig. 1.

The innovative wing box conceived for the inner front wing (IFW) and the RW consists of a main tubular spar running through the quarter-chord; a rear nonstructural spar running through the 3/4 local chord; very lightweight and rigid ribs connecting the two spars and a nonstructural, very thin and transparent plastic film wing covering. A high-strength carbon/epoxy composite material is used for spar design. The main tubular spar is a cylindrical tube to be manufactured by means of a filament winding technique with two bonded caps for flexural stiffness. The LE is made of a plastic material whereas the TE is made with foam.

A single-spar wing box for the outer wing (OW) and a two-spar wing box for the fin, both entirely made with a carbon/epoxy composite material are adopted.

Table 1 HAPD design speeds

V_S, m/s	V_A, m/s	V_C, m/s	V_D, m/s
14.07	28.94	33.30	39.00

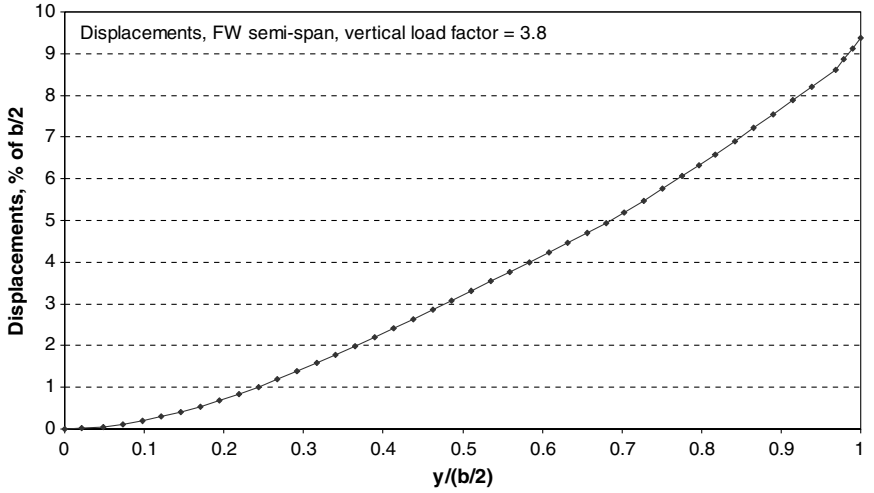

Fig. 2 HAPD, FW semispan displacements.

The fuselage main structure is composed of frames, stringers, and a structural floor plate in the ventral zone, all made of a high-strength aluminum alloy (AA); the nose is made of a plastic material whereas the aft body is of carbon/epoxy composite material.

The RW is joined to the apex of the vertical tail unit (VTU). The VTU and FW are joined to the fuselage in two different sections.

Three numerical models of the airplane have to be developed to evaluate the aerodynamic derivatives. A dynamic model for the symmetrical normal modes calculation; an aerodynamic model; and a so-called interface model (IM) that represents the link between the first two models. The IM is made up of a set of grids on which aerodynamic loads, inertia loads, and modal displacements are transferred.

Geometric structural nonlinearities can be considered negligible because the deformations experienced during balanced maneuver analyses at maximum vertical load factor are quite close to the values typically attained during a balanced maneuver of a large conventional aircraft (about 10% of the semispan). The following figure (Fig. 2) shows the maximum displacements at each station along the FW semispan of HAPD.

A. Dynamic Model

A dynamic model for the semi-airplane has been developed with the aid of MacNeal–Schwendler Corporation (MSC) Nastran software. Suitable constraint sets are introduced in the plane of symmetry xz to reproduce symmetrical flight conditions.

By means of a semi-automatic mesh generation a reasonably accurate structural model of the wings has been generated with a relatively little effort. The fuselage model, as well as the wing junctions and the fin model, resulting from a rather detailed structural design process, are integrated into the global model.

The inner FW and RW cylindrical spar models are made of beam elements (PBEAM and PBEAML property entries), whereas plate elements are adopted to simulate the LE and the TE structures (PSHELL entries). The outer wing model together with the winglet and the fin models, are made of beam elements for the spar caps, plate elements for the structural wing covering (PCOMP entries) and for LE and TE structures (PSHELL entries). Concentrated masses (CONM2 entry) are used to reproduce the wing inertia distribution. The inertia behavior of control surfaces is simulated by means of DMIG mass matrices, for which a two nodes scheme is adopted.

Fuselage frames and stringers are modeled with bar elements (PBAR entries), whereas the ventral floor plate is modeled with plate elements (PSHELL entries). The aft body structure together with the nose are simulated using plate elements (PSHELL and PCOMP entries). The inertia distribution along the x axis is reproduced by means of four groups of concentrated masses (CONM2 elements).

The wing junction is made up of two elements: a lower part having a barrel shape, connecting the inner and the outer FW, and an upper

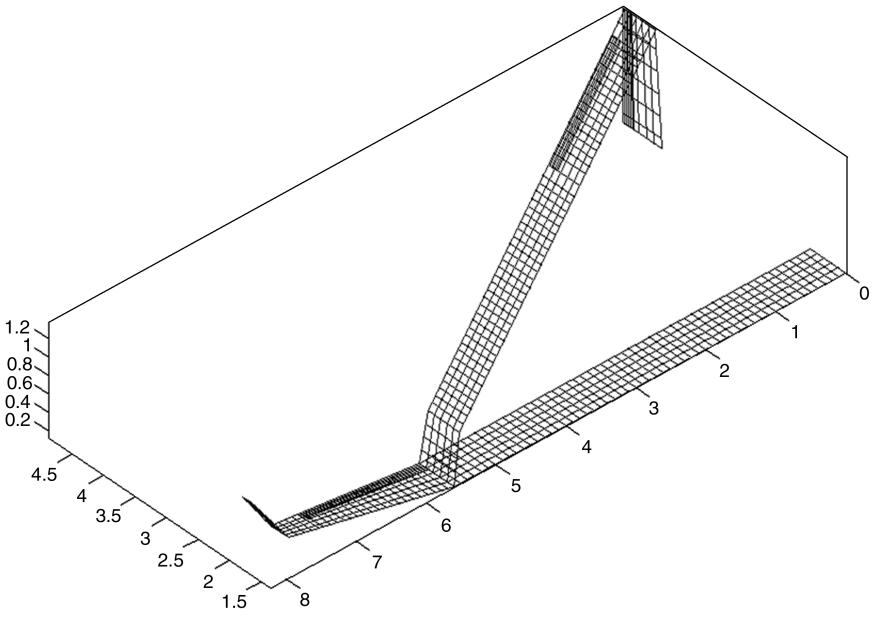

Fig. 3 DLM aerodynamic model.

part having a typical wing box type structure connecting FW and RW. The whole structure is designed using a high-strength carbon/epoxy composite material. The dynamic model of the wing junction makes use of plate elements (PCOMP entries) and CONM2 elements for the nonstructural masses.

The rear junction connects RW to the fin, it is made up of a machined frame in AA. The rear junction is replaced in the global dynamic model by two equivalent DMIG matrices simulating its structural and inertia behavior.

B. Aerodynamic Model

The aerodynamic analyses are carried out by using a linear panel method, the doublet lattice method (DLM), based on the pulsating doublet theory.

DLM was developed by Albano and Rodden in 1969 [37], it is based on the linearized theory of the aerodynamic potential. The freestream is considered uniform but it can be steady or harmonically variable. DLM can be used as an aerodynamic load evaluator for aeroelastic purposes in a fast, reliable and relatively simple way, especially if compared with more modern unsteady aerodynamic solvers, such as those based on the direct integration of Navier–Stokes equations.

The aerodynamic model is made up of 940 aerodynamic boxes. Figure 3 shows how the aerodynamic mesh is more refined on flight-control surfaces and in their neighborhood, to perform more accurate calculations. The aerodynamics of the fuselage has not been accounted for because of its very slight influence on the symmetric aerodynamic behavior of the entire airplane resulting from computational fluid dynamics (CFD) calculations.

All aerodynamic analyses are executed by taking into account airfoil cambers and aerodynamic corrections due to viscous effects because the aerodynamic model has been calibrated at zero angle of attack by means of comparison with CFD calculations. Such a correction has been performed by imposing $C_{n'}$ and $C_{m'}$ distributions obtained through integration of the aerodynamic pressures coming from CFD. The equivalent pressures on the aerodynamic boxes are adopted as aerodynamic zero effect.

C. Interface Model

To transfer the data between dynamic and aerodynamic models, a link between a set of master grids belonging to the dynamic model (interchange data grids, or IDGs) and all aerodynamic boxes is created. This link is guaranteed by using spline type and bilinear type interpolation operators [38].

All 6 degrees of freedom of IDGs are constrained to the dynamic model through RBE2 elements (for each RBE2 element, the master grid coincides with the associated IDG).

Figure 4 shows the geometric superposition of aerodynamic model and IDGs.

D. Aerodynamic Derivatives

The evaluation of the Aerodynamic Derivatives is carried out by using a modal approach, typical of the dynamic aeroelasticity domain.

Normal modes are used extensively in the dynamic analyses of airplane responses, including investigations into aeroelastic instabilities such as flutter. Extensive calculations (Nastran) have to be carried out to estimate the normal modes and their associated natural frequencies of a generic unrestrained airplane. With the respect to a conventional approach, the principal advantage is that it is possible to solve a generic structural static problem without fixing suitable constraints to make the problem isostatic: the airplane can be considered unrestrained. Furthermore, because the normal modes are available, there is benefit to be gained from using them for static problems as well as for dynamic problems and so unifying the approaches to static and dynamic aeroelasticity. This is an important aspect if a load alleviation is implemented when considering unsteady maneuvers.

The general equation of the dynamic aeroelasticity in a modal approach in the frequency domain, for a symmetric maneuver is:

$$\left\{(j\omega)^2\begin{bmatrix}\underline{\underline{m}}_{RR} & 0\\ 0 & \underline{\underline{m}}_{EE}\end{bmatrix}+(j\omega)\begin{bmatrix}0 & 0\\ 0 & \underline{\underline{\sigma}}_{EE}\end{bmatrix}+\begin{bmatrix}0 & 0\\ 0 & \underline{\underline{K}}_{EE}\end{bmatrix}\right\}\begin{bmatrix}\underline{q}_R(j\omega)\\ \underline{q}_E(j\omega)\end{bmatrix}=\frac{1}{2}\rho V^2\begin{bmatrix}\underline{\underline{Q}}_{RR} & \underline{\underline{Q}}_{RE}\\ \underline{\underline{Q}}_{ER} & \underline{\underline{Q}}_{EE}\end{bmatrix}\begin{bmatrix}\underline{q}_R(j\omega)\\ \underline{q}_E(j\omega)\end{bmatrix}+\frac{1}{2}\rho V^2\begin{bmatrix}\underline{q}_{R\delta}\\ \underline{q}_{E\delta}\end{bmatrix}\delta(j\omega) \tag{6}$$

where single and double underlines denote, respectively, vectors and tensors. Equation (6) is written by distinguishing the rigid modes from the elastic ones through subscripts R and S, the components of $\underline{q}_R$ are the degrees of freedom of the rigid airplane: the plunge and the pitch mode

$$\underline{q}_R=\begin{pmatrix}h\\ \theta\end{pmatrix}=\begin{cases}\text{Plunge}\\ \text{Pitch}\end{cases} \tag{7}$$

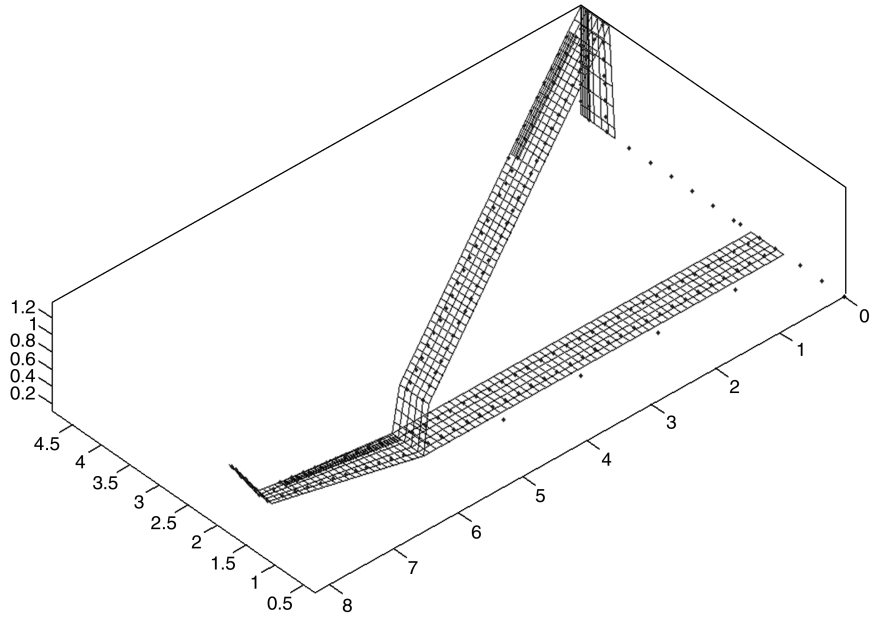

Fig. 4 Geometric superposition of aerodynamic and interface model.

The quasi-steady aerodynamic pressures are determined by adopting a quadratic approximation of the unsteady pressures obtained from DLM calculations

$$\underline{\tilde{P}}(jk) = \underline{\underline{P}}_0 + jk\underline{\underline{P}}_1 + (jk)^2\underline{\underline{P}}_2 \tag{8}$$

Because quasi-steady aerodynamic pressures are interpolated on the IM, for each normal mode shape, the quasi-steady generalized aerodynamic forces $\underline{\underline{Q}}$ are evaluated as follows:

$$\frac{1}{2}\rho V^2\underline{\underline{Q}}\,\underline{q} = \frac{1}{2}\rho V^2\underline{\underline{\Phi}}^T\cdot\underline{\underline{\Delta S}}\cdot\underline{\tilde{P}}(jk)\cdot\underline{q} = \frac{1}{2}\rho V^2\underline{\underline{\Phi}}^T\cdot\underline{\underline{\Delta S}}\cdot[\underline{\underline{P}}_0 + jk\underline{\underline{P}}_1 + (jk)^2\underline{\underline{P}}_2]\cdot\underline{q} \tag{9}$$

$$\frac{1}{2}\rho V^2\underline{\underline{Q}}\,\underline{q} = \frac{1}{2}\rho V^2\underline{\underline{G}}_0\cdot\underline{q}(t) + \frac{1}{2}\rho V c_r\underline{\underline{G}}_1\cdot\dot{\underline{q}}(t) + \frac{1}{2}\rho c_r^2\underline{\underline{G}}_2\cdot\ddot{\underline{q}}(t) \tag{10}$$

where

$$\begin{cases} \underline{\underline{G}}_0 = \underline{\underline{\Phi}}^T\cdot\underline{\underline{\Delta S}}\cdot\underline{\underline{P}}_0 \\ \underline{\underline{G}}_2 = \underline{\underline{\Phi}}^T\cdot\underline{\underline{\Delta S}}\cdot\underline{\underline{P}}_2 \\ \underline{\underline{G}}_2 = \underline{\underline{\Phi}}^T\cdot\underline{\underline{\Delta S}}\cdot\underline{\underline{P}}_2 \\ j\omega\underline{q} = \dot{\underline{q}}(t);\ (j\omega)^2\underline{q} = \ddot{\underline{q}}(t) \end{cases} \tag{11}$$

and

$$k = \frac{\omega c_r}{V} \tag{12}$$

is the reduced frequency.

The quasi-steady aerodynamic pressures are evaluated for the following two values of the reduced frequency

$$k = 0 \qquad k = \varepsilon \tag{13}$$

with ε very close to zero. By substituting Eq. (13) in Eq. (8) one gets

$$\underline{\tilde{P}}(0) = \underline{\underline{P}}_0 \qquad \underline{\tilde{P}}(j\varepsilon) = \underline{\underline{P}}_r + j\underline{\underline{P}}_i = \underline{\underline{P}}_0 + j\varepsilon\underline{\underline{P}}_1 + (j\varepsilon)^2\underline{\underline{P}}_2 \tag{14}$$

where the subscripts r and i mean real and imaginary part of the aerodynamic pressures at the reduced frequency equal to ε.

From Eq. (14) it follows:

$$\underline{\underline{P}}_0 = \underline{\tilde{P}}(0) \qquad \underline{\underline{P}}_1 = 1/\varepsilon\underline{\underline{P}}_i(\varepsilon) \qquad \underline{\underline{P}}_2 = \left(\frac{1}{\varepsilon^2}\right)(\underline{\tilde{P}}(0) - \underline{\underline{P}}_r(\varepsilon)) \tag{15}$$

from which $\underline{\tilde{P}}(jk)$ and $\underline{\underline{Q}}$ are determined.

Under the hypothesis of quasi-steady conditions, for $\varepsilon \ll 1$, Eq. (10) becomes

$$\frac{1}{2}\rho V^2\underline{\underline{Q}}\,\underline{q} = \frac{1}{2}\rho V^2[\underline{\underline{G}}_0 + jk\underline{\underline{G}}_1]\underline{q} = \eta_0\underline{\underline{G}}_0\underline{q} + \eta_1\underline{\underline{G}}_1\dot{\underline{q}} \tag{16}$$

with $\eta_0 = \frac{1}{2}\rho V^2$; $\eta_1 = \frac{1}{2}\rho Vc$.

Equation (6), written in the time domain, becomes:

$$\begin{bmatrix} \underline{\underline{m}}_{RR} & 0 \\ 0 & \underline{\underline{m}}_{EE} \end{bmatrix}\begin{pmatrix} \ddot{\underline{q}}_R \\ \ddot{\underline{q}}_E \end{pmatrix} + \begin{bmatrix} 0 & 0 \\ 0 & \underline{\underline{\sigma}}_{EE} \end{bmatrix}\begin{pmatrix} \dot{\underline{q}}_R \\ \dot{\underline{q}}_E \end{pmatrix} + \begin{bmatrix} 0 & 0 \\ 0 & \underline{\underline{K}}_{EE} \end{bmatrix}\begin{pmatrix} \underline{q}_R \\ \underline{q}_E \end{pmatrix} = \begin{bmatrix} \eta_0\underline{\underline{G}}_{0,RR}\underline{q}_R + \eta_1\underline{\underline{G}}_{1,RR}\dot{\underline{q}}_R & \eta_0\underline{\underline{G}}_{0,RE}\underline{q}_E + \eta_1\underline{\underline{G}}_{1,RR}\dot{\underline{q}}_E \\ \eta_0\underline{\underline{G}}_{0,ER}\underline{q}_R + \eta_1\underline{\underline{G}}_{1,ER}\dot{\underline{q}}_R & \eta_0\underline{\underline{G}}_{0,EE}\underline{q}_E + \eta_1\underline{\underline{G}}_{1,EE}\dot{\underline{q}}_E \end{bmatrix} + \begin{bmatrix} \eta_0\underline{\underline{G}}_{0,R\delta}\delta + \eta_1\underline{\underline{G}}_{1,R\delta}\dot{\delta} \\ \eta_0\underline{\underline{G}}_{0,E\delta}\delta + \eta_1\underline{\underline{G}}_{1,E\delta}\dot{\delta} \end{bmatrix} \tag{17}$$

With the assumption of negligibility of: 1) elastic accelerations with the respect to rigid ones, 2) elastic velocities with the respect to rigid ones, and 3) control speed with the respect to control deflection, it is possible to simplify Eq. (17) as follows:

$$\underline{\underline{m}}_{RR}\ddot{\underline{q}}_R = \eta_1\underline{\underline{G}}_{1,RR}\dot{\underline{q}}_R + \eta_0\underline{\underline{G}}_{0,RR}\dot{\underline{q}}_R + \eta_0\underline{\underline{G}}_{0,R\delta}\delta + \eta_0\underline{\underline{G}}_{0,RE}\underline{q}_E + \eta_0\underline{\underline{G}}_{0,Rq} + \underline{F}_{R\text{ext}} \tag{18}$$

$$(\underline{\underline{K}}_{EE} - \eta_0\underline{\underline{G}}_{0,EE})\underline{q}_E = \eta_0\underline{\underline{G}}_{0,ER}\underline{q}_R + \eta_1\underline{\underline{G}}_{1,ER}\dot{\underline{q}}_R + \eta_0\underline{\underline{G}}_{0,E\delta}\delta + \eta_0\underline{\underline{G}}_{0,Eq} + \underline{F}_{E\text{ext}} \tag{19}$$

In Eqs. (18) and (19), the aerodynamic terms depending exclusively on the dynamic pressure ($\eta_0\underline{\underline{G}}_{0,Rq}$ and $\eta_0\underline{\underline{G}}_{0,Eq}$) and the terms representing possible external forces (i.e., engine trust) $\underline{F}_{R\text{ext}}$ and $\underline{F}_{E\text{ext}}$ have been taken into account.

By defining the following equalities:

$$\begin{gathered} \underline{\underline{A}}_{1,RR} = \eta_1\underline{\underline{G}}_{1,RR} \qquad \underline{\underline{A}}_{0,RR} = \eta_0\underline{\underline{G}}_{0,RR} \qquad \underline{\underline{A}}_{0,RE} = \eta_0\underline{\underline{G}}_{0,RE} \\ \underline{F}_{0,RC} = \eta_0\underline{\underline{G}}_{0,R\delta} \qquad \underline{F}_{0,Rq} = \eta_0\underline{\underline{G}}_{0,Rq}; \qquad \underline{\tilde{K}} = (\underline{\underline{K}}_{EE} - \eta_0\underline{\underline{G}}_{0,EE}) \\ \underline{F}_{0,ER} = \eta_0\underline{\tilde{K}}^{-1}\underline{\underline{G}}_{0,ER} \qquad \underline{F}_{1,ER} = \eta_1\underline{\tilde{K}}^{-1}\underline{\underline{G}}_{1,ER} \\ \underline{F}_{0,EC} = \eta_0\underline{\tilde{K}}^{-1}\underline{G}_{0,E\delta} \qquad \underline{F}_{0,Eq} = \eta_0\underline{\tilde{K}}^{-1}\underline{G}_{0,Eq} \qquad \underline{F}_{0E\text{ext}} = \underline{\tilde{K}}^{-1}\underline{F}_{E\text{ext}} \end{gathered} \tag{20}$$

Equations (18) and (19) become:

$$\underline{\underline{m}}_{RR}\ddot{\underline{q}}_R = \underline{\underline{A}}_{0,RR}q_R + \underline{\underline{A}}_{1,RR}\dot{\underline{q}}_R + \underline{\underline{A}}_{0,RE}q_E + \underline{F}_{0,RC}\delta + \underline{F}_{0,Rq} + \underline{F}_{R\text{ext}} \tag{21}$$

$$\underline{q}_E = \underline{\underline{F}}_{0,ER}\underline{q}_R + \underline{\underline{F}}_{1,ER}\dot{\underline{q}}_R + \underline{F}_{0,EC}\delta + \underline{F}_{0,Eq} + \underline{F}_{0E\text{ext}} \tag{22}$$

By substituting Eq. (22) into Eq. (21), a second-order differential equation system is obtained:

$$\underline{\underline{m}}_{RR}\ddot{\underline{q}}_R + \underline{\hat{C}}_{RR}\dot{\underline{q}}_R + \underline{\hat{K}}_{RR}\underline{q}_R = \underline{F}_{\text{ext}q} + \underline{F}_{\text{ext}0} + \underline{F}_C\delta(t) \tag{23}$$

where

$$\begin{cases} \underline{\hat{K}}_{RR} = -(\underline{\underline{A}}_{0,RR} + \underline{\underline{A}}_{0,RE}\underline{\underline{F}}_{0,ER}) \\ \underline{\hat{C}}_{RR} = -(\underline{\underline{A}}_{1,RR} + \underline{\underline{A}}_{1,RE}\underline{\underline{F}}_{1,ER}) \\ \underline{F}_{\text{ext}q} = \underline{F}_{0,Rq} + \underline{\underline{A}}_{0,RE}\underline{F}_{0,Eq} \\ \underline{F}_C = \underline{F}_{0,RC} + \underline{\underline{A}}_{0,RE}\underline{F}_{0,EC} \\ \underline{F}_{\text{ext}0} = \underline{F}_{R\text{ext}} + \underline{\underline{A}}_{0,RE}\underline{F}_{0E\text{ext}} \end{cases} \tag{24}$$

With the previous assumptions, the general equation of the dynamic aeroelasticity, a system of N differential equations, becomes a system of two differential equations of motion (rigid degrees of freedom only) plus N-2 algebraic equations, uncoupled from the first ones. Equation (23), together with Eq. (22), are the main equations in the symmetric quasi-steady aeroelasticity, from which it is possible to determine the evolution of a symmetric maneuver during time or to evaluate the parameters of a balanced and steady symmetric maneuver.

The aerodynamic derivatives are calculated as follows: depending on the aeroelastic properties of the airplane in terms of modal characteristics and quasi-steady aerodynamics, the terms $\underline{\underline{F}}_{0,ER}$, $\underline{\underline{F}}_{1,ER}$, $\underline{F}_{0,EC}$, $\underline{F}_{0,Eq}$, $\underline{F}_{0E\text{ext}}$ are calculated as shown previously.

The elastic modal degrees of freedom $\underline{q}_E$ are determined for each unit aerodynamic condition (including unit control surface deflections) by putting in Eq. (22) the different sets of $\underline{q}_R$, δ, etc., representative of each unit aerodynamic contribution.

The aerodynamic forces on each box are:

$$\underline{F}_{\text{aero}}(\hat{t}) = \frac{1}{2}\rho V^2\underline{\underline{\Delta S}}\,\underline{\tilde{P}}(\hat{t})\underline{q}(\hat{t}) = \frac{1}{2}\rho V^2\underline{\underline{\Delta S}}\left(\underline{\underline{P}}_0\underline{q}(\hat{t}) + \underline{\underline{P}}_1\dot{\underline{q}}(\hat{t})\frac{c}{V}\right) \tag{25}$$

where $\underline{\underline{\Delta S}}$ is the diagonal matrix of the aerodynamic box areas.

By representing the aerodynamic pressures in their explicit form (zero effect, control surface deflection effect, and the effect due to elastic and rigid modal degrees of freedom), Eq. (25) becomes:

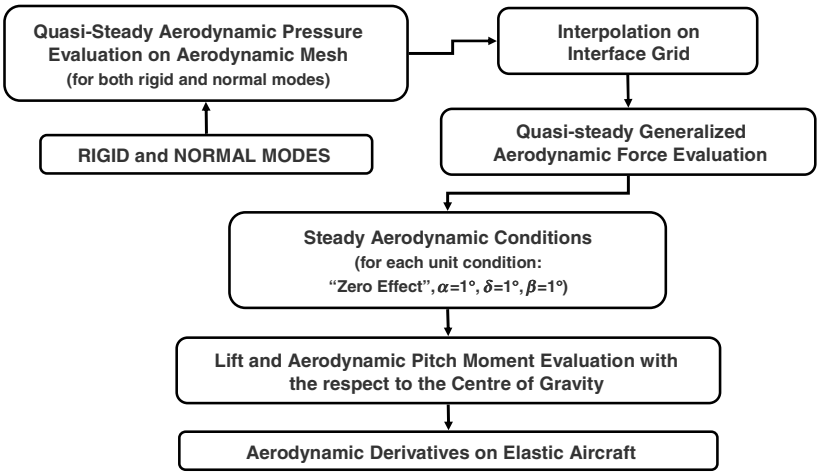

Fig. 5 Aerodynamic derivatives calculation taking into account aeroelastic effects.

$$\underline{F}_{\text{aero}}(\hat{t}) = \frac{1}{2}\rho V^2 \underline{\underline{\Delta S}}\left(\underline{\underline{P}}_{0R}\underline{q}_R(\hat{t}) + \underline{\underline{P}}_{0E}\underline{q}_E(\hat{t}) + \underline{\underline{P}}_{1R}\dot{\underline{q}}_R(\hat{t})\frac{c}{V}\right) + \frac{1}{2}\rho V^2 \underline{\underline{\Delta S}}[\underline{P}_q + \underline{P}_\delta \delta(\hat{t})] \tag{26}$$

The resultant lift and pitching moment, evaluated by integrating the aerodynamic forces of Eq. (26) calculated for each aerodynamic contribution (and for all the flight conditions of interest in terms of Mach number, altitude, and dynamic pressure) are just the aerodynamic lift and pitching moment derivatives.

Figure 5 shows a schematic of the whole process.

E. Load Derivatives

In the case of airplanes having a conventional configuration, the main structure of the wing can be considered statically determinate. The load derivatives (or bending moment derivatives) have to be calculated through integration of the aerodynamic pressure due to each unit aerodynamic load contribution and of single forces and concentrated moments due to the unit inertia load condition.

In the case of airplanes having an unconventional configuration such as a joined-wing one, the main structure is redundant. Under this hypothesis it is not possible to calculate the internal load characteristics by means of a simple integration of the external load distribution because the internal stresses are strictly dependent on the stiffness behavior of the structure. Consequently, it is necessary to solve the static problem by applying the external loads and a suitable constraint set to make the problem isostatic. Then the internal load characteristics are evaluated through integration of the internal nodal forces, resulting from the finite element force balance (grid point forces balance, GPFORCE, [39]).

The static problem is solved with the aid of MSC Nastran by loading the structural model with each unit aerodynamic and inertia load contribution. The unit bending moment distributions and thus the bending moment derivatives are evaluated by integrating the GPFORCE resulting from the postprocessing performed with MSC Patran. Figure 6 summarizes the process.

F. Input Data and Derivatives Calculation

Because of specific requirements related to Guidance, Navigation, and Control, HAPD has ten flight-control surfaces: four ailerons, four elevators, and two rudders.

The control surfaces used as load alleviators are the inner ailerons, and the wing control section used for monitoring the principal bending moment in the front wing root station as illustrated in Fig. 7.

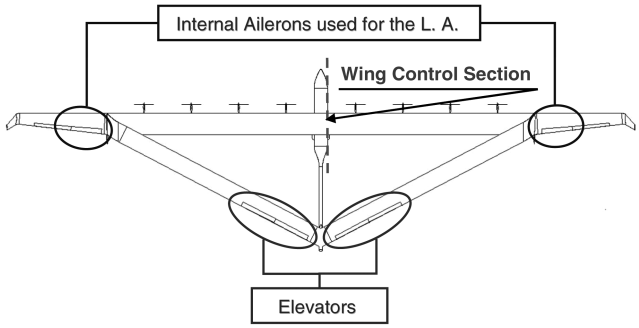

Fig. 7 HAPD flight-control surfaces and WCS.

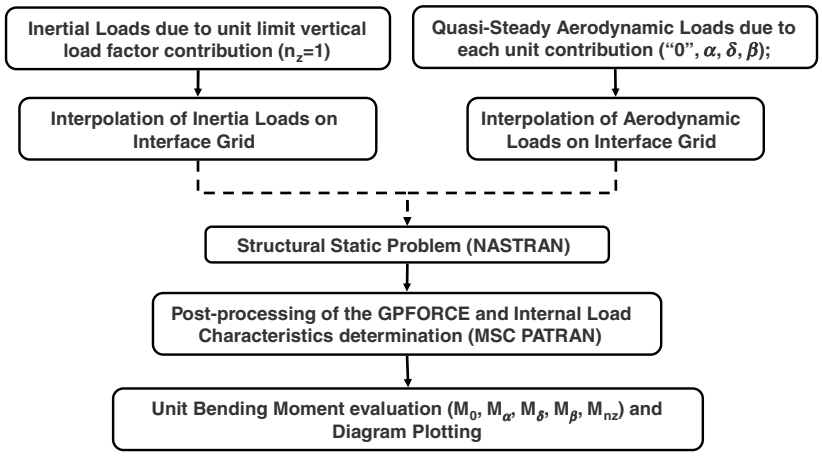

Fig. 6 Bending moment derivatives calculation for an aircraft in a nonconventional configuration (joined wing).

Table 2 Calculation data, aerodynamic and load derivatives

V, m/s	Mach	ρ, kg/m^3	q, Pa	
33.30	0.00	1.23	679.20	
C_{z0}	$C_{z\alpha}$, 1/deg	$C_{z\delta}$, 1/deg	$C_{z\beta}$, 1/deg	
0.3458	0.0785	0.0071	0.0002	
C_{m0}	$C_{m\alpha}$, 1/deg	$C_{m\delta}$, 1/deg	$C_{m\beta}$, 1/deg	
0.1398	−0.06021	−0.0210	−0.00005	
M_0, Nm	M_α, Nm/deg	M_δ, Nm/deg	M_β, Nm/deg	M_{nz}, Nm
3389.38	660.71	28.3	17.49	−1589.26

The calculations are carried out for different values of aircraft speed from the design maneuvering speed to the dive speed, at sea level, for a vertical load factor variable between 1.0 and 3.8. Because of the quite regular behavior of the test aircraft under load alleviation, in this paper only the calculations involving the design cruising speed are reported. All derivatives are evaluated taking into account the structural flexibility according to the above illustrated method, at the dynamic pressures reported in Table 2.

Input calculation data, lift and moment aerodynamic derivatives, together with bending moment derivatives are also reported in Table 2.

G. Results

Different levels of load alleviation are performed to establish a relationship between flight parameters such as α, β, δ, the vertical load factor n_z, and the AF.

Flight parameters together with the control function G of Eq. (5) are plotted both against the vertical load factor parameterized with AF and against AF parameterized with the vertical load factor (Figs. 8 and 9).

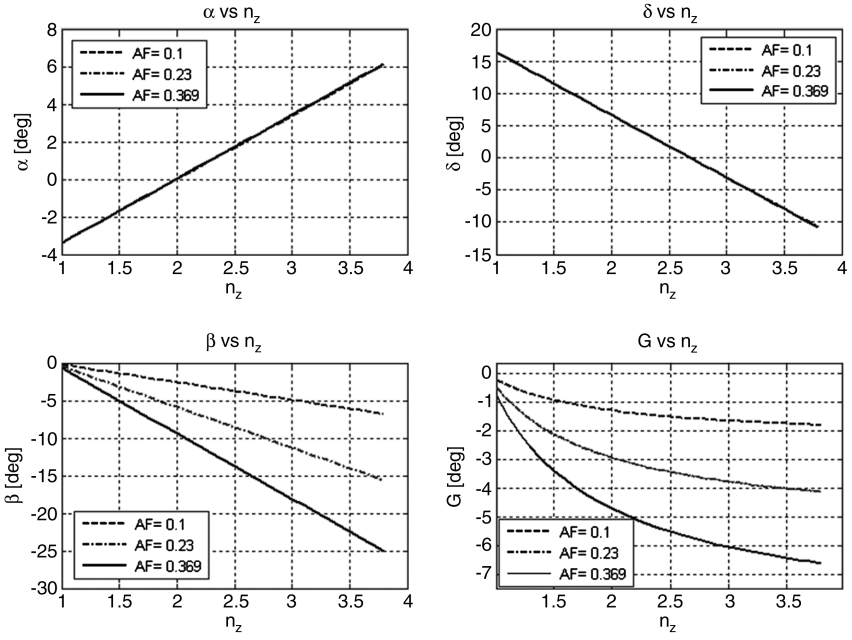

Fig. 8 Attitude, elevator deflection, aileron deflection, and control function vs vertical load factor.

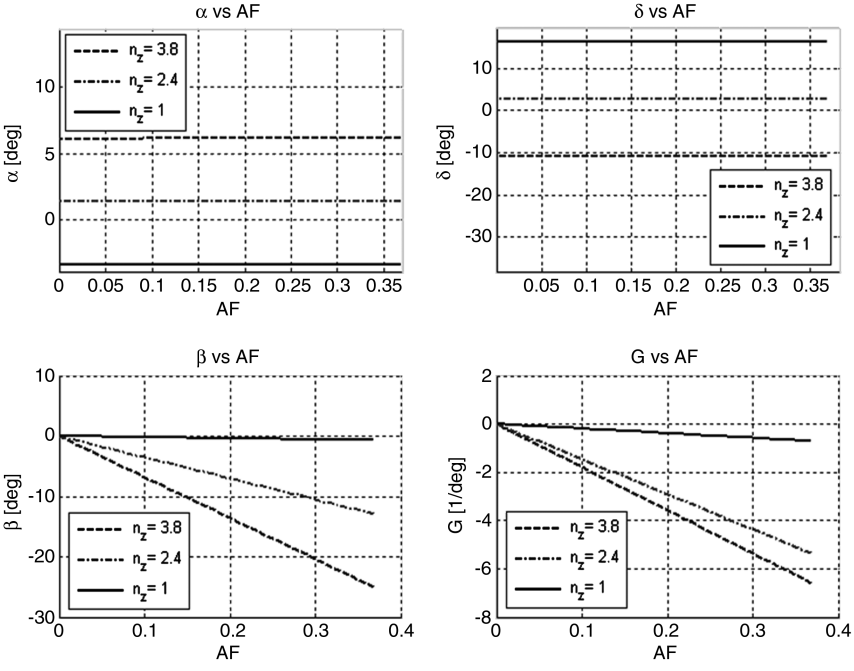

Fig. 9 Attitude, elevator deflection, aileron deflection, and control function vs AF.

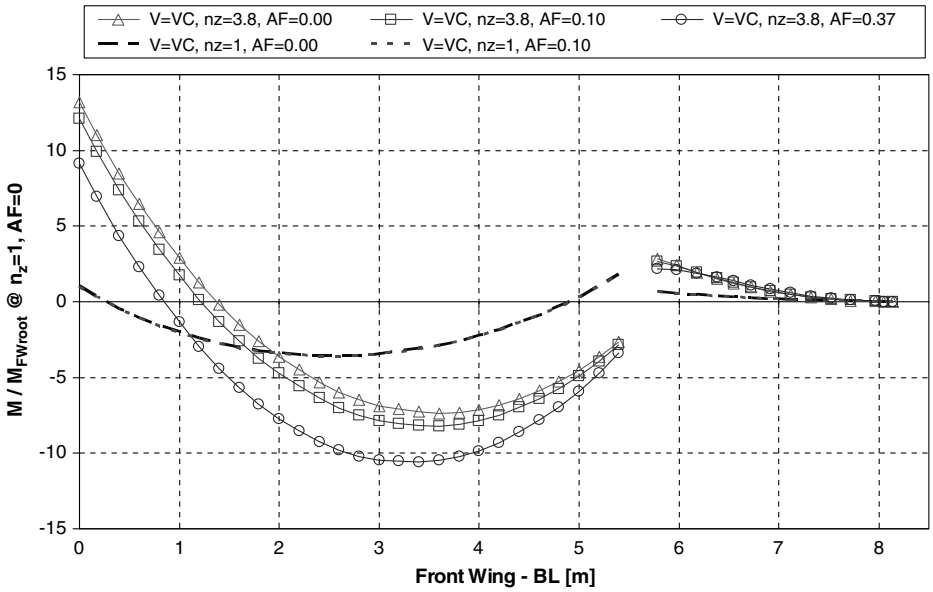

Fig. 10 Bending moment distribution on the FW normalized with the respect to the principal bending moment at FW root at $n_z = 1$ and AF = 0 (AF = [0.00, 0.10, 0.37], n_z = [1.0, 3.8], sea level).

Figures 8 and 9 show that if n_z increases the load alleviator deflection β linearly decreases; furthermore the stronger the drop in β the higher the value of AF. Hence, the maximum attainable value of AF (and thus of the alleviation level) is bounded by the maximum deflection of the ailerons. AF = 0.37 is chosen as maximum value because it produces, at the maximum vertical load factor, an inner aileron deflection of 25 deg that is the largest allowable value of the load alleviator deflection.

Calculations performed at V_A, not reported in this paper for reasons of conciseness, result in an increase of the angle of attack α with the respect to n_z and AF. Also in this case the higher the rise of α with the respect of n_z the higher is the value of AF. This behavior leads to an important conclusion: the adoption of a load alleviator that induces a positive aerodynamic pitch derivative ($C_{m\beta} = 0.00143$), typical of the airplanes having a negative sweep angle wing, makes this method not applicable in high-lift conditions, such as at the point V_A of the maneuver diagram. In such a situation, with the aircraft at its maximum attitude, the activation of the load alleviation system may lead to aircraft stall.

Instead, when the load alleviator induces a negative or zero aerodynamic pitch derivative, typical of the airplanes having a positive sweep angle wing, a negative and symmetric actuation of the control surfaces does not produce an increase in the angle of attack. Such a situation can also occur because of aeroelastic effects, as well as in the results presented herein (Figs. 8 and 9), for which the elastic deformation of the wing modifies the aerodynamic behavior induced by the control surfaces as load alleviators, leading to a $C_{m\beta}$ practically equal to zero. In this case the elevator deflection does not vary with the respect to AF.

Nevertheless, if at the point V_A of the maneuver diagram the load alleviator is such that $C_{m\beta} < 0$, then the illustrated load alleviation method can be applied also at high-lift conditions.

Calculations performed using this method give a set of diagrams of the control function G with the respect to n_z, AF, Mach number and dynamic pressure. Such an abacus can be viewed as an indication for the preliminary design of a control system aimed at controlling the load alleviation in real time, i.e., by adopting the values of G as a first estimation of the controller gain. Otherwise, starting from the values of the airplane derivatives with the respect to the dynamic pressure and the Mach number actually measured in flight, a computer system calculating in real time the function G can be designed and engineered as an inboard system.

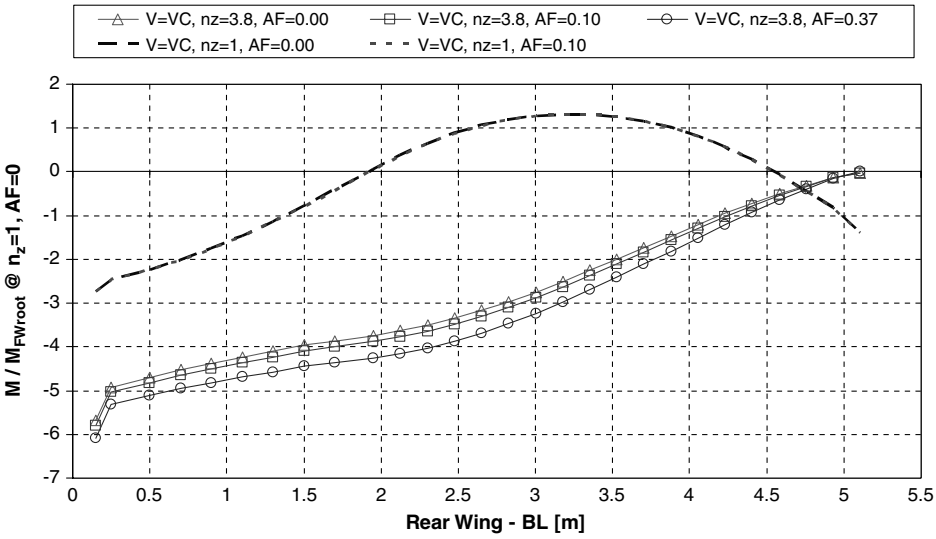

Fig. 11 Bending moment distribution on the RW normalized with the respect to the principal bending moment at FW root at $n_z = 1$ and AF = 0 (AF = [0.00, 0.10, 0.37], n_z = [1.0, 3.8], sea level).

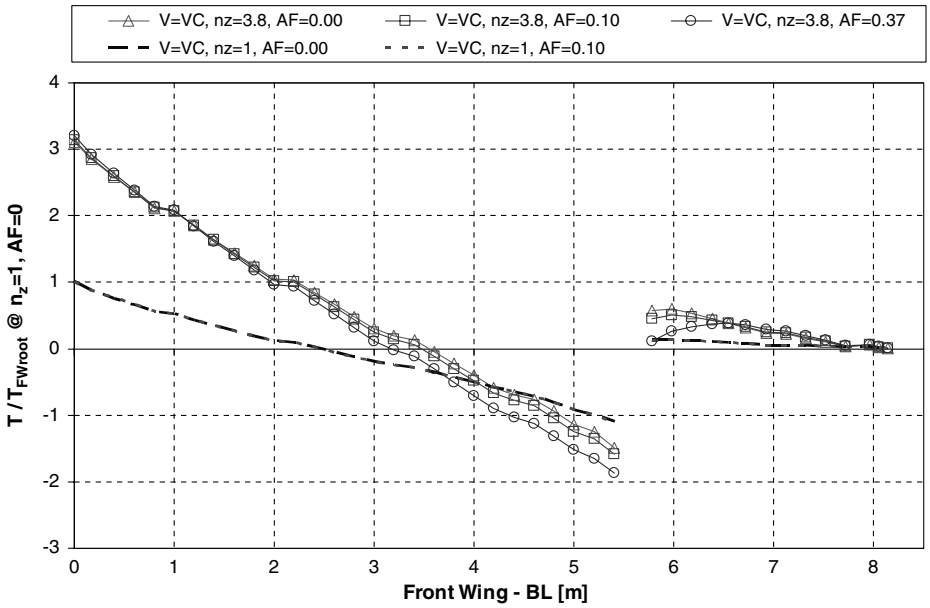

Fig. 12 Shear distribution on the FW normalized with the respect to the principal shear at FW root $n_z = 1$ and AF = 0 (AF = [0.00, 0.10, 0.37], n_z = [1.0, 3.8], sea level).

Starting from the unit bending moment and shear distributions for each unit aerodynamic and inertial contribution, and combining them together with the flight parameters shown above, the bending moment distribution on the entire wing system of the aircraft can be plotted for different values of n_z and AF. For the sake of clarity, the bending moment distributions on FW (Fig. 10) and RW (Fig. 11) are normalized with the respect to the value of the bending moment at the FW root at $n_z = 1.0$ and AF = 0.0. Again, evaluating the unit shear distributions for each unit aerodynamic and inertial contribution, and combining them together with the previous flight parameters, the principal shear distribution on the front and rear wings of the aircraft can be plotted for different values of n_z and AF.

Figure 10 shows that for both $n_z = 1$ and $n_z = 3.8$, an important decrease of the bending moment on WCS is obtained. For AF = 0.37 and $n_z = 3.8$ a decrease of the bending moment at center wing section (BL = 0) equal to 30% (normalized with the respect to the bending moment evaluated on the FW root at $n_z = 1.0$ without any load alleviation system (AF = 0.0)), is also experienced.

For the RW (Fig. 11), for both $n_z = 1$ and $n_z = 3.8$, even having different bending moment distribution shapes, there is a decrease of principal bending moment at the wing root. Nevertheless, in this case, there is no benefit to be gained from this trend because the bending moment increases in absolute value.

Furthermore both Figs. 10 and 11 show a generalized drop of bending moment throughout the whole wing system, from the inner aileron location up to the wing root. It should be noted that the overall decrease in bending moment could result in a local increase (in absolute value) far from WCS, close to the inner FW half span. Moreover, the higher the imposed alleviation factor, the stronger the bending moment increasing far from WCS, thus resulting in a significant limitation to the alleviation. As a result, during the design phase, the absence of local structural failures has to be assured.

Figure 12 shows that there is a slight shear increasing with respect to the bending moment reduction on WCS. Instead, Fig. 13 shows that at the RW root there is a reduction of principal shear (an increase in absolute value). This behavior is peculiar to an unconventional configuration such as the joined-wing one. Conversely, for a cantilever wing configuration, even if the load alleviator is activated, the principal shear on the wing root must be constant (the load factor is kept constant). For an aircraft having a joined-wing configuration,

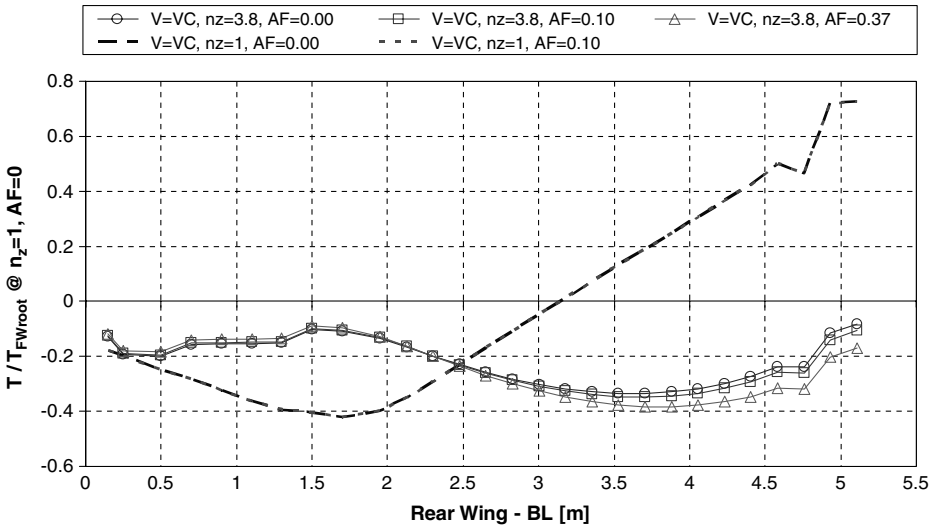

Fig. 13 Shear distribution on the RW normalized with the respect to the principal shear at FW root at $n_z = 1$ and AF = 0 (AF = [0.00, 0.10, 0.37], n_z = [1.0, 3.8], sea level).

the increase in angle of attack, as a consequence of the load alleviator deflection, produces a rearranging of the aerodynamic load with a subsequent redistribution of internal load characteristics. Because the FW is stiffer, the load augmentation on the FW is higher than on the RW.

IV. Conclusions

A formulation for a symmetric and balanced maneuvering load alleviation taking into account the aircraft flexibility has been derived. Starting from the linear system (4), it has been illustrated how it is possible to obtain a desired value of the bending moment alleviation in a generic fixed wing station close to the wing root. To solve the system (4) in a specific flight condition (depending on vertical load factor, dynamic pressure, and Mach number), the aerodynamic and load derivatives of the airplane must be calculated. A method to determine such derivatives of an aircraft in an unconventional configuration such as a joined-wing one, using a modal approach and taking into account aeroelastic effects, has been presented.

The hypothesis of linear aerodynamics leads to a decomposition of the aerodynamic forces making possible the evaluation of the aerodynamic derivatives. The hypotheses of linear structure and unvarying tensor of inertia are supported both by the literature [26] and by the structural behavior of the airplane leading to small structural displacements under limit loads. Moreover, the load derivatives are calculated by adopting a method conceived for joined-wing configurations and mainly based on the structural linearity.

The application to the joined-wing unmanned aircraft HAPD has been carried out.

Having once evaluated the unit shear and bending moment distributions for each unit aerodynamic and inertial contribution, and combining them together with the flight parameters resulting from the solution of the load alleviation system (4), the load characteristic distributions can be plotted for different values of n_z and AF. Figures 10 and 11 show that an important reduction of the bending can be gained, especially in the case of high aspect ratio and nonnegligible structural flexibility. For the test-case aircraft, an increase of the maximum attainable value of AF with the respect to the dynamic pressure has been observed although the load distribution over the FW and the RW varies because of rising aeroelastic effects (AF varies from 0.19 at V_A to 0.37 at V_C at sea level).

A limitation of the method is its inapplicability in high-lift conditions, such as those falling between the points V_S and V_A of the maneuver diagram, at the vertical limit load factor, in the case of a positive value of $C_{m\beta}$. In such a situation, with the aircraft at its maximum attitude, the activation of the load alleviation system may produce aircraft stall. Another limitation consists in the uncontrollability of the internal load far from WCS, that requires extensive calculations to a prevent sudden load increase with consequent unexpected structural failures.

Furthermore, Figs. 8 and 9 are examples of how is possible to obtain, for each value of dynamic pressure and Mach number, a control function abacus yielding the change of G with the respect to n_z and AF. Such an abacus can be viewed as an indication for the preliminary design of a control system aimed at controlling the load alleviation in real time, during an unsteady longitudinal maneuver; G is a first estimation of the gain to be used in a SISO system to link the vertical load factor (output) to the load alleviator deflection (input).

As a further experimental implication, knowing the airplane derivatives for a given the dynamic pressure and the Mach number measured in flight, a computer system can be designed and engineered as an inboard system aimed at calculating the function G in real time (for a desired value of AF) hence the associated load alleviator deflection for the correct reduction wing bending.

For all the aspects explained above, benefits can be gained from integrating such a system on HAPD: expected fatigue life extension (reflecting on the reusability) and structural weight reduction resulting in greater payloads (scientific test devices) for more accurate flight tests and/or better ground observation missions.

Acknowledgments

The work has been performed within a research project aimed at the preliminary design of a high-altitude performance demonstrator funded by the Italian Ministry of Instruction, University and Research through the Italian Aerospace Research Program in development at CIRA, The Italian Aerospace Research Center.

This study is part of the activity related to a Philosophy Doctorate in Aerospace Engineering at the University of Naples "Federico II" (Italy).

Many thanks to Leonardo Lecce at the University of Naples "Federico II" (Italy) for his precious advice during the draft of this paper.

References

[1] Hahn, K.-U., and Koenig, R., "Attas Flight Test and Simulation Results of the Advanced Gust Management System Lars," *AIAA Atmospheric Flight Mechanics Conference*, AIAA, Washington, D.C., 1992.

[2] Merat, R., "Study of a Direct Lift Control System Based on the A380 Aircraft," *46th AIAA Aerospace Sciences Meeting and Exhibit*, AIAA, Reston, VA, 2008.

[3] Wildschek, A., Maier, R., Hromcik, M., Hanis, T., Schirrer, A., Kozek, M., Westermayer, C., and Hemedi, M., "Hybrid Controller For Gust Load Alleviation and Ride Comfort Improvement Using Direct Lift Control Flaps," *3rd European Conference For Aerospace Sciences (EUCASS)*, The European Conference for AeroSpace Sciences, Versailles, France, 2009.

[4] Hecker, S., and Hahn, K.-U., "Advanced Gust Load Alleviation System for Large Flexible Aircraft," *1st CEAS European Air & Space Conference*, CEAS, Berlin, Germany, 2007.

[5] Pratt, K. G., "A Survey of Active Controls Benefits to Supersonic Transport," *Symposium on Advanced Control Technology*, NASA, July 1974.

[6] Kurzhals, P. R., "Active Controls in Aircraft Design: Executive Summary," *FMP Symposium on Stability and Control*, AGARD, Oct. 1978.

[7] Caplin, J., Ray, A., and Joshi, S., "Damage-Mitigating Control of Aircraft for Enhanced Structural Durability," *IEEE Transactions on Aerospace and Electronic Systems*, Vol. 37, No. 3, July 2001, pp. 849–862.
doi:10.1109/7.953241

[8] "Selected Advanced Aerodynamics and Active Control Technology Concepts Development on a Derivative B-747 Aircraft," NASA 3164, July 1982.

[9] White, R. J., "Improving the Airplane Efficiency by Use of Wing Maneuver Load Alleviation," *Journal of Aircraft*, Vol. 8, No. 10, 1971, pp. 769, 775.
doi:10.2514/3.59169

[10] Woods–Vedeler, J. A., Pototzky, A. S., and Hoadley, S. T., "Rolling Maneuver Load Alleviation Using Active Controls," *Journal of Aircraft*, Vol. 32, No. 1, Jan.–Feb. 1995, pp. 68–76.
doi:10.2514/3.46685

[11] Harpoothian, E., and Oswald, W. B., "Use of Ailerons to Reduce Wing Loads," U.S. Pat. 2,742,245, Douglas Aircraft Co., Santa Monica, CA, 1949.

[12] Rogers, J. T., and Manning, K. J. R., "Wing Load Alleviation System Using Tabbed Aileron," U.S. Patent No. 4'479'620, The Boeing Company, Seattle, WA, Oct. 1984.

[13] Lewis, G. E., "Maneuver Load Alleviation System," U.S. Patent No. 4'796'192, The Boeing Company, Seattle, WA, Jan. 1989.

[14] Romeo, G., Frulla, G., and Cestino, E., "Design of a High-Altitude Long-Endurance Solar-Powered Unmanned Air Vehicle for Multi-Payload and Operations," *Journal of Aerospace Engineering*, Vol. 221, Part G, pp. 199–216.
doi:10.1243/09544100JAERO119

[15] Hall, D. W., and Hall, S. A., "Structural Sizing of a Solar Powered Aircraft," NASA CR-172313, 1984.

[16] Colozza, A., and Dolce, J. L., "High-Altitude, Long-Endurance Airships for Coastal Surveillance," NASA TM-2005-213427.

[17] Nickol, C. L., Guynn, M. D., Kohout, L. L., and Ozoroski, T. A., "High Altitude Long Endurance Air Vehicle Analysis of Alternatives and Technology Requirements Development," *45th AIAA Aerospace Sciences Meeting and Exhibit*, AIAA, Reston, VA, 2007.

[18] Romeo, G., Frulla, G., Cestino, E., and Corsino, G., "HELIPLAT: Design, Aerodynamic, Structural Analysis of Long-Endurance Solar-Powered Stratospheric Platform," *Journal of Aircraft*, Vol. 41, No. 6, Nov.–Dec. 2004, pp. 1505–1520.

doi:10.2514/1.2723

[19] Patil, M. J., Hodges, D. H., and Cesnik, C. E. S., "Nonlinear Aeroelasticity and Flight Dynamics of High-Altitude Long-Endurance Aircraft," *Journal of Aircraft*, Vol. 38, No. 1, 2001, pp. 88–94. doi:10.2514/2.2738

[20] Patil, M. J., and Hodges, D. H., "Flight Dynamics of Highly Flexible Flying Wings," *Journal of Aircraft*, Vol. 43, No. 6, 2006, pp. 1790–1799. doi:10.2514/1.17640

[21] Raghavan, B., and Patil, M. J., "Flight Dynamics of High-Aspect-Ratio Flying Wings: Effect of Large Trim Deformation," *Journal of Aircraft*, Vol. 46, No. 5, 2009, pp. 1808–1812. doi:10.2514/1.36847

[22] Patil, M. J., "Nonlinear Gust Response of Highly Flexible Aircraft," *48th AIAA/ASME/ASCE/AHS/ASC Structures, Structural Dynamics, and Materials Conference*, AIAA, Reston, VA, 2007.

[23] Shearer, C. M., and Cesnik, C. E. S., "Nonlinear Flight Dynamics of Very Flexible Aircraft," *Journal of Aircraft*, Vol. 44, No. 5, 2007, pp. 1528–1545. doi:10.2514/1.27606

[24] Cesnik, C. E. S., and Brown, E. L., "Modeling of High Aspect Ratio Active Flexible Wings for Roll Control," *Proceedings of the 43rd AIAA/ASME/ASCE/AHS Structures, Structural Dynamics, and Materials Conferences*, Denver, CO, AIAA 2002-1719, 2002.

[25] Cesnik, C. E. S., and Brown, E. L., "Active Wing Warping Control of a Joined-Wing Airplane Configuration," *Proceedings of the 44th AIAA/ASME/ASCE/AHS Structures, Structural Dynamics, and Materials Conferences*, Norfolk, VA, AIAA 2003-1715, 2003.

[26] Patil, M. J., "Nonlinear Aeroelastic Analysis of Joined-Wing Aircraft," *44th AIAA/ASME/ASCE/AHS/ASC Structures, Structural Dynamics & Materials Conference*, AIAA, Reston, VA, 2003.

[27] Wolkovitch, J., "The Joined-Wing: An Overview," *The AIAA 23rd Aerospace Sciences Meeting*, AIAA, New York, 1986.

[28] Gallman, J. W., and Smith, S. C., "Optimization of Joined Wing Aircraft," *Journal of Aircraft*, Vol. 30, No. 6, Nov.–Dec. 1993, pp. 897–905. doi:10.2514/3.46432

[29] Di Palma, L., Paletta, N., and Pecora, M., "Aeroelastic Desing of a Joined Wing UAV," *SAE 2009 AeroTech Congress & Exhibition*, Society of Automotive Engineers, Warrendale, PA, Nov. 2009.

[30] Frediani, A., Rizzo, E., Bottoni, C., Scanu, J., and Iezzi, G., "The Prandtl Plane Aircraft Configuration," *Aeronautics Days*, Vienna, Austria, June 2006.

[31] Frediani, A., "The Prandtl Wing," Von Karman Institute, Lecture Series on Innovative Configuration and Advanced Concepts for Future Civil Aircraft, June 2005.

[32] Dal Canto, D., Divoux, N., Frediani, A., Ghiringhelli, G. L., and Terraneo, M., "Preliminary Design Against Flutter of a PrandtlPlane Lifting System," *XX Congresso Nazionale AIDAA, Milano*, Associazione Italiana di Aeronautica e Astronautica, Milan, 2009.

[33] Bindolino, G., Ghiringhelli, G., Ricci, S., and Terraneo, M., "Multilevel Structural Optimization for Preliminary Wing-Box Weight Estimation," *Journal of Aircraft*, Vol. 47, No. 2, March–April 2010, pp. 475, 489. doi:10.2514/1.41552

[34] Demasi, L., and Livne, E., "Exploratory Studies of Joined Wing Aeroelasticity," *46th AIAA/ASME/ASCE/AHS/ASC Structures, Structural Dynamics, and Materials Conference*, AIAA Paper 2005-2172, 2005.

[35] Demasi, L., and Livne, E., "Dynamic Aeroelasticity Coupling Full Order Geometrically Nonlinear Structures and Full Order Linear Unsteady Aerodynamics: The Joined Wing Case," *49th AIAA/ASME/ASCE/AHS/ASC Structures, Structural Dynamics, and Materials Conference*, AIAA Paper 2008-1818, 2008.

[36] Imperatore, B., and Vecchione, L., "A Flexible Wing Unmanned Aerial Research System," *SAE 2009 AeroTech Congress & Exhibition*, Society of Automotive Engineers, Warrendale, PA, Nov. 2009.

[37] Albano, E., and Rodden, W. P., "A Doublet-Lattice Method for Calculating Lift Distributions on Oscillating Surfaces in Subsonic Flows," *AIAA Journal*, Vol. 7, No. 2, Feb. 1969, pp. 279–285. doi:10.2514/3.5086

[38] Harden, R. L., and Desmarais, R. N., "Interpolation Using Surface Splines," *Journal of Aircraft*, Vol. 9, No. 2, Feb. 1972, pp. 189–191. doi:10.2514/3.44330

[39] The MacNeal–Schwendler Corporation, "MSC/Nastran Version 70.5–Quick Reference Guide," Feb. 1998.